Title
Structural studies of lithium insertion in lithium manganese oxides

Journal
Intercalation Compounds for Battery Materials; Proceedings of the Electrochemical Society, 99(24)

Authors
Horne, Craig R.
Bergmann, Uwe
Grush, Melissa M.
et al.

Publication Date
2000

Structural Studies of Lithium Insertion in Lithium Manganese Oxides

C.R. Horne[1,2,*], U. Bergmann[1], M.M. Grush[3], J. Kim[4], A. Manthiram[4], S.P. Cramer[1,5], K.A. Striebel[1], and E.J. Cairns[1,2]

1. Lawrence Berkeley National Laboratory, Berkeley, CA 94720
2. University of California, Berkeley, CA 94720
3. University of Tennessee, Knoxville, TN 37996
4. The University of Texas at Austin, Austin, TX 78712
5. University of California, Davis, CA 95616

The cubic spinel $LiMn_2O_4$ is attractive as a positive electrode active material in lithium rechargeable batteries due to its low cost, low toxicity and high specific energy (1,2). However, excessive capacity fading has limited the widespread commercialization of batteries containing $LiMn_2O_4$. It has been widely shown that this material transforms into a tetragonal phase upon lithium insertion past one ion per formula unit, i.e. $x > 1$ in $Li_xMn_2O_4$ (1). The transformation has been attributed to the Jahn-Teller effect (1,THAC14). One capacity fade mechanism in this material concerns the large volume expansion associated with this transformation. The expansion is problematic as both cubic and tetragonal phases coexist. Particle fracture results, creating isolated pieces of electrochemically inactive material within the positive electrode (WEN1, 4). Additionally, measurements of the lithium diffusion coefficient reported in the literature have shown that the lithium chemical diffusion coefficient decreases when $x > 1$ (5, STRI#). An explanation for this behavior is not readily apparent from an atomic structure

* present address: NanoGram Corporation, Fremont, CA 94538

point of view since the Li^+ diffusion pathway is similar for both phases (through octahedral-tetragonal-octahedral sites), the unit cell volume is larger in t-$Li_xMn_2O_4$, and vacancies for Li^+ transport exist on both octahedral and tetrahedral sites within each compositional region (1,THAC13,THAC14). Recently, an alternative lithium manganese oxide, $Li_{1.5}Na_{0.5}MnI_{0.12}O_{2.84}$, has been synthesized and shown to possess good cycling stability (6). This material is an amorphous form synthesized at low temperatures using a simple solution technique.

Lithium ion insertion requires accommodation of an accompanying electron within the host's structure to maintain charge neutrality. Therefore, to properly investigate the structural reaction mechanism occurring during lithium insertion in $LiMn_2O_4$ requires characterization of the electronic as well as the atomic structure. To this end we performed X-ray diffraction (XRD) to determine the long range atomic structure (phase purity and lattice parameters), as well as an array of X-ray spectroscopic techniques: Mn K-edge X-ray Absorption Near-Edge Spectroscopy (XANES) and Extended X-ray Absorption Fine Structure (EXAFS), Mn Kβ X-ray Emission Spectroscopy (XES), Mn L-edge XANES, and Mn L-edge XES. The absorption spectroscopies, XANES and EXAFS, are sensitive to the local atomic structure: bond distances, coordination, and symmetry. Conversely, the emission spectroscopies are sensitive to several aspects of the electronic structure: oxidation state and degree of covalency.

EXPERIMENTAL

Two samples of $LiMn_2O_4$, one from Chemetal, Inc. and the other synthesized in our laboratory, were characterized as well as described in reference HORN2. The synthesis and characterization of chemically delithiated and lithiated derivatives of $LiMn_2O_4$ as

well as the Mn^{3+} tetragonal spinels $MgMn_2O_4$ and $ZnMn_2O_4$ are also described in reference HORN2. In addition to $LiMn_2O_4$ spinel-based samples, $Li_{1.5}Na_{0.5}MnI_{0.12}O_{2.84}$ and electrodes containing $Li_{1.5}Na_{0.5}MnI_{0.12}O_{2.84}$ were studied. Electrodes were extracted from cells cycled 40 times galvanostatically at 0.5 mA/cm^2; one electrode was left in the charged state whereas the other was left in the discharged state. References 6 contains more detail on the synthesis of $Li_{1.5}Na_{0.5}MnI_{0.12}O_{2.84}$ along with cell fabrication and testing.

Mn K-edge XANES and EXAFS was performed on Beamline 2-3 at the Stanford Synchrotron Light Source as described in references HORN1 and HORN2. Mn Kβ XES was performed using a high-resolution spectrometer containing Si(220) crystal analyzers (BERG#) on Beamline X-25 at the National Synchrotron Light Source. Mn L-edge XANES was performed on Beamline 6.3.2 at the Advanced Light Source. Mn L-edge XES was performed on Beamline 8.0 at the Advanced Light Source; procedures used for data collection and analysis are described in reference HORN2.

RESULTS AND DISCUSSION

Based upon measurements of the magnetic moment (MASQ1) as well as the fact that it is a small-polaron conductor (SHEF1,GUAN@), $LiMn_2O_4$ can be classified as a type II mixed-valent compound containing an equal fraction of Mn^{3+} and Mn^{4+} (COX2). EXAFS measurements on $LiMn_2O_4$ revealed that the best fit for Mn coordination was with a split first shell, one sub-shell containing five oxygen atoms and another sub-shell, at a longer distance, containing one oxygen atom (i.e. a 5+1 coordination). This counters the expectation of six oxygen due to the cubic symmetry of $LiMn_2O_4$. However, a dynamic Jahn-Teller of the $[Mn^{3+}O_6]$ octahedra, surmised in references 1 and THAC14,

yields four short and two long Mn^{3+}-O bonds (i.e a 4+2 coordination). Combining the four short Mn^{3+}-O bonds with the six Mn^{4+}-O bonds results in an average coordination of (5+1) as discussed in reference HORN1. A recent paper (YAMA1) has tried to rationalize the presence of distorted $[Mn^{3+}O_6]$ octahedra within the cubic spinel with a disproportionation scheme. However, a small-polaron conduction mechanism (COX2) and the low-temperature transformation of cubic $LiMn_2O_4$ to a pure orthorhombic phase (20#) suggests that the two Mn species are interspersed. Resolving the EXAFS results with these other physical properties leads us to the structural interpretation shown in Figure 1 where the $[Mn^{3+}O_6]$ and $[Mn^{4+}O_6]$ octahedra are adjacent. The $[Mn^{3+}O_6]$ octahedra undergo a ferrodistortive dynamic JTE whereas the $[Mn^{4+}O_6]$ rotate to maintain cubic symmetry; temporally and spatially averaged cubic symmetry result.

High-resolution Kβ XES, demonstrated as a bulk probe of Mn oxidation state (CRAM5, BERG$) was performed on $Li_xMn_2O_4$, $0.1 < x \leq 2.0$. Identical results were achieved on samples synthesized both chemically and electrochemically. Upon delithiation the $K\beta_{1,3}$ peak shifted towards lower energy indicating oxidation of the Mn^{3+} to Mn^{4+} occurs. Conversely, the $K\beta_{1,3}$ peak shifted towards higher energy upon lithiation indicating that the Mn^{4+} are reduced to high-spin Mn^{3+} (HORN1). Peak positions for the end compositions (i.e. $x \leq 0.2$ and $x = 2.0$) matched well to Mn^{4+} and high-spin Mn^{3+} model compounds (CRAM5). The spectral shifts in Mn $L_{II,III}$-edge XANES were consistent with the $K\beta_{1,3}$ results.

Mn K-edge XANES was also performed on the set of chemically and electrochemically prepared $Li_xMn_2O_4$, $0.1 < x \leq 2.0$. Again, identical results were obtained. Figure 2 (left) is a comparison of the Mn K-edge XANES from chemically

delithiated and lithiated spinels with $LiMn_2O_4$. The changes occurring upon delithiation are consistent with the $K\beta_{1,3}$ and $L_{II,III}$-edge XANES results. In addition to displaying peak shifts to lower energy as expected with Mn^{4+} reduction, the K-edge XANES of the lithiated spinel $Li_2Mn_2O_4$ possesses a prominent step in the edge. Figure 2 (right) compares the Mn K-edge XANES from $Li_2Mn_2O_4$ and two "model" Mn^{3+} tetragonal spinels with similar $[MnO_6]$ octahedra distortion parameters, $MgMn_2O_4$ and $ZnMn_2O_4$. Instead of a step, both model spinel Mn K-edge XANES possess a shoulder in the edge, consistent with a distortion parameter in the range of all three compounds, 1.14 to 1.16. Note that the pre-edge regions for all three oxides, enlarged in Figure 2 (right), are similar. Garcia *et al.* (GARC2) has shown that as the octahedral distortion parameter increases a low energy shoulder first appears in the edge, changing into a step at a distortion parameter equal to approximately 1.3, described as a square-planar coordination.

Recently, Shadle *et al.* showed that a step in the edge can be attributed to a 1*s* -> 4*p* + LMCT shakedown (ligand to metal charge transfer) transition arising from increased covalency (SHAD*). The covalency manifests when an increased stabilization of the metal 3*d* level induces electron transfer from the ligand. To ascertain if $Li_2Mn_2O_4$ possesses a larger covalency than $MgMn_2O_4$ and $ZnMn_2O_4$ the $L\alpha/L\beta$ ratio of the Mn L-edge XES was determined for each oxide. Grush *et al.* have recently shown that a 1% increase in the Mn $L\alpha/L\beta$ ratio correlates to a 1.6% increase in covalency (GRUS1). Figure 3 contains the Mn L-edge XES for the three oxides with the calculated $L\alpha/L\beta$ ratios shown in the inset. The data in Figure 3 reveal that a significantly larger degree of covalency exists in $Li_2Mn_2O_4$. Considering that all three oxides possess nearly identical

[MnO_6] octahedra leads to the conclusion that the covalency results from the inserted Li^+ residing within the 8*d* site of $Li_2Mn_2O_4$ (THAC13); this site is empty in both $MgMn_2O_4$ and $ZnMn_2O_4$.

Mn K-edge XANES was performed on $Li_{1.5}Na_{0.5}MnO_{2.85}I_{0.12}$ along with two electrodes to compare how electronic structure changes induced by changing lithium content within crystalline and amorphous lithium-manganese oxides. The XANES of all three $Li_{1.5}Na_{0.5}MnO_{2.85}I_{0.12}$ based samples described in the Experimental section are shown in Figure 4; the pre-edge region for each of the respective spectra are magnified by a factor of 5. Comparing the $Li_{1.5}Na_{0.5}MnO_{2.85}I_{0.12}$ powder XANES shape to those in Figure 2 (left) reveals that the Mn are octahedrally coordinated, presumably by oxygen, with a Mn oxidation state close to +4. The slightly lower main peak energy in the $Li_{1.5}Na_{0.5}MnO_{2.85}I_{0.12}$ powder could be due to the slightly lower Mn oxidation state, a larger Mn-O bond length, and/or a more covalent Mn-O bond (HORN6). Another observation is that the rising edge for the $Li_{1.5}Na_{0.5}MnO_{2.85}I_{0.12}$ powder is smoother than that of λ-MnO_2 suggesting that the [MnO_6] octahedral bond angles are less distorted than those for λ-MnO_2 or $LiMn_2O_4$ (HORN6).

Comparing the powder XANES with the cycled, discharged XANES elucidates the effects of lithiating $Li_{1.5}Na_{0.5}MnO_{2.85}I_{0.12}$. As is the case with the spinel system, upon discharging, the edge moves to lower energy, consistent with reduction of the Mn^{4+} in $Li_{1.5}Na_{0.5}MnO_{2.85}I_{0.12}$ by the electron-compensating insertion of a Li^+. The fact that the pre-edge region of the cycled, discharged electrode XANES is similar to those of the tetragonal Mn^{3+} spinels in Figure 2 (right) implies that the [MnO_6]octahedra become distorted during lithiation. However, the smaller difference between main peak and edge

shoulder energies compared to $MgMn_2O_4$ and $ZnMn_2O_4$ suggests that the distortion parameter of discharged $Li_{1.5}Na_{0.5}MnO_{2.85}I_{0.12}$ is not as large (HORN6). The data of Figure 4, in particular the pre-edge regions, show that the powder and cycled, charged electrode possess comparable characteristics; this suggests that the local structure is not grossly altered by repeated cycling. Thus the distortion observed upon lithiating $Li_{1.5}Na_{0.5}MnO_{2.85}I_{0.12}$ is not as destructive, compared with the spinel system, to the structural integrity which explains the superior cycling stability. Lastly the differences among the cycled, discharged $Li_{1.5}Na_{0.5}MnO_{2.85}I_{0.12}$ and $Li_2Mn_2O_4$ XANES indicate that lithiation of the amorphous oxide does not cause increased covalence as found within the spinel system. Therefore, it would be expected that $Li_{1.5}Na_{0.5}MnO_{2.85}I_{0.12}$ possesses faster Li^+ transport over the lower voltage region.

CONCLUSIONS

The spectroscopic studies revealed that high-spin $[Mn^{3+}O_6]$ octahedra are present in $LiMn_2O_4$ and undergo a dynamic Jahn-Teller effect in the parent spinel. The presence of distorted $[Mn^{3+}O_6]$ octahedra within the cubic spinel structure was rationalized within a ferrodistortive model. Additionally, it was found that the electron accompanying lithium insertion is accommodated at the Mn site. These three attributes are needed to ascribe the the cooperative Jahn-Teller effect as the mechanism for the cubic to tetragonal transformation taking place upon lithiating $LiMn_2O_4$. Therefore, the energy balance of the transformation is described with the following equation:

Eq. 1. $$\Delta G^{c/t} = -\Delta G_V V^t_{(Mn^{3+})} + A\,g^{c/t} + \Delta G_S V^t_{(Mn^{4+})}.$$

A comparison to tetragonal Mn^{3+} spinels revealed that the degree of covalency increases in the lithiated spinel. The further stabilization of electronic energy levels due to increased covalence is concomitant with the cooperative Jahn-Teller effect.

The signatures of increased covalence were not found in the amorphous lithium manganese oxide. Additionally, the distortion parameter of this material's lithiated derivative was found to be less than that for the spinel. These results indicate that lithiation of $Li_{1.5}Na_{0.5}MnI_{0.12}O_{2.84}$ occurs with a lesser effect on atomic and electronic structure as compared to the crystalline spinel. These differences are attributed to the improved cyclability exhibited by the amorphous material.

ACKNOWLEDGEMENTS

The work at Lawrence Berkeley National Laboratory was supported by the Director, Office of Energy Research, Office of Basic Energy Sciences, Chemical Sciences Division of the U.S. Department of Energy under Contract No. DE-AC03-76SF00098 to the Ernest Orlando Lawrence Berkeley National Laboratory. The work at The University of Texas at Austin was supported by the National Science Foundation Grant DMR-9401999

REFERENCES

1. M.M. Thackeray, W.I.F. David, P.G. Bruce and J.B. Goodenough, Mat. Res. Bull., **18**, 461 (1983).

2. J.M. Tarascon and D. Guyomard, Electrochem. Acta, **38**, 1221 (1993).

3. R.J. Gummow, A. de Kock, and M.M. Thackeray, Sol. St. Ionics, **69**, 59 (1994).

4. M.M. Thackeray, Y. Shao-Horn, A.J. Kahaian, K.D. Kepler, E. Skinner, J.T. Vaughey, and S.A. Hackney, Electrochem. Sol. St. Lett., **1**, 7 (1998).

5. J. Barker, R. Pynenburg, and R. Koksbang, J. Power Sources, **52**, 185 (1994).

6. J. Kim and A. Manthiram, Nature, **390**, 265 (1997).

20#. K. Oikawa, T. Kamiyama, F. Izumi, B. Chakoumakos, H. Ituka, M. Wakihara, J. Li, and Y. Matsui, Solid State Ionics **109**, 35 (1998).

BERG#. U. Bergmann and S.P. Cramer, *SPIE Proc*., **3448**(1998)198.

BERG$. U. Bergmann, C.R. Horne, T.J. Collins, J.M. Workman, and S.P. Cramer, *Chem. Phys. Lett*., **302**(1999)119.

CRAM5. G. Peng, F.M.F. deGroot, K. Hämäläinen, J.A. Moore, X. Wang, M.M. Grush, J.B. Hastings, D.P. Siddons, W.H. Armstrong, O.C. Mullins and S.P. Cramer, *J. Am. Chem. Soc.*, **116**, 2914 (1994).

COX2. Cox, P.A. The Electronic Structure of Solids, Oxford University Press, Oxford **1988**.

GARC2. J. Garcia, A. Bianconi, M. Benfatto, and C.R. Natoli, *J. Physique*, **47** (1986) C8-49.

GRUS1. Grush, M.M.; Muramatsu, Y.; Underwood, J.H., Gullikson, E.M.; Ederer, D.L.; Perera, R.C.C.; Callcot, T.A. *J. Elect. Spect.* **1998** 92, 225.

GUAN@. J. Guan and M. Liu, *Solid State Ionics*, **110**(1998)21.

HORN1. E.J. Cairns, C.R. Horne, B.J. Weiss, M.M. Grush, and S.P. Cramer, in Proceedings of the 2nd International Symposium on New Materials for Fuel Cells and Modern Battery Systems, Montreal, Canada, July 6-10, 1997. O. Savadago and P.R. Roberge, eds., École Polytechnique de Montreal. 1997. p. 336.

HORN2. C.R. Horne, U. Bergmann, M.M. Grush, E.J. Cairns, and S.P. Cramer, submitted to *J. Phys. Chem. B.*

HORN6. C.R. Horne, U. Bergmann, J. Kim, K.A. Streibel, A. Manthiram, S.P. Cramer,

and E.J. Cairns, submitted to *J. Electrochem. Soc.*

MASQ1. C. Masquelier, M. Tabuchi, K. Ado, R. Kanno, Y. Kobayashi, Y. Maki, O. Nakamura, and J. B. Goodenough, *J. Sol. St. Chem.*, **123** (1996) 255.

SHAD*. Shadle, S.E. ; Penner-Hahn, J.E.; Schugar, H.J.; Hedman, B.; Hodgson, K.O.; Solomon, E.I. *J. Am. Chem. Soc.* **1993** 115, 767.

SHEF1. Sheftel, I.T.; Pavlotskii, Y.V. *Inorg. Mater. (USSR)* **1966** 2, 918.

STRI#. K.S. Striebel, A. Rougier, C.R. Horne, R.P. Reade, and E.J. Cairns, *J. Electrochem. Soc.*, Accepted.

THAC13. W. I. F. David, M. M. Thackeray, L.A. De Picciotto and J. B. Goodenough, *J. Sol. State Chem.*, **67** (1987) 316.

THAC14. J.B. Goodenough, M.M. Thackeray, W.I.F. David and P.G. Bruce, *Rev. de Chem. Min.*, **21** (1984) 435.

WEN1 S. J. Wen, T. J. Richardson, L. Ma, K. A. Striebel, P. N. Ross, and E. J. Cairns, *J. Electrochem. Soc.*, **143** (1996) L136.

YAMA#. H. Yamaguchi, A. Yamada, and H. Uwe, *Phys. Rev. B* **1998** 58, 8.

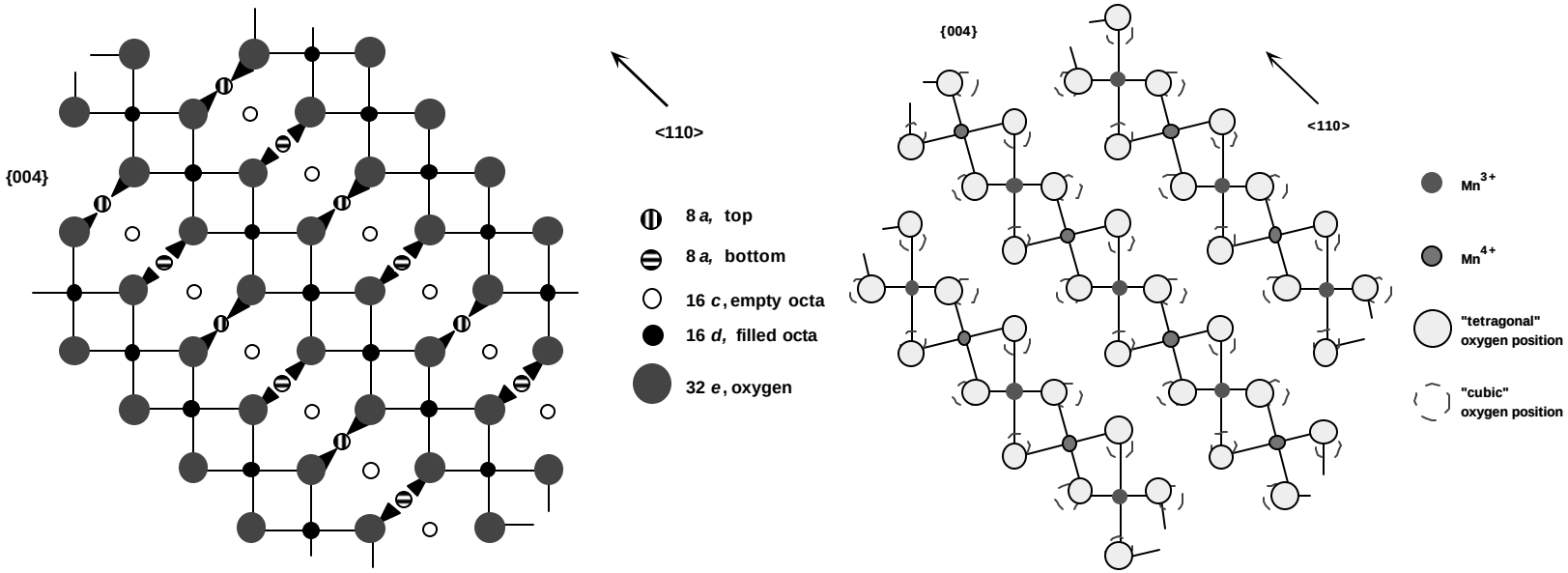

Figure 1. (left) Schematic of cubic spinel lattice showing {004} plane; 8*a* sites are just above and below the plane. (right) Schematic of $LiMn_2O_4$ {004} plane incorporating dynamically-distorted $[Mn^{3+}O_6]$ octahedra and undistorted $[Mn^{4+}O_6]$ octahedra.

* present address: NanoGram Corporation, Fremont, CA 94538

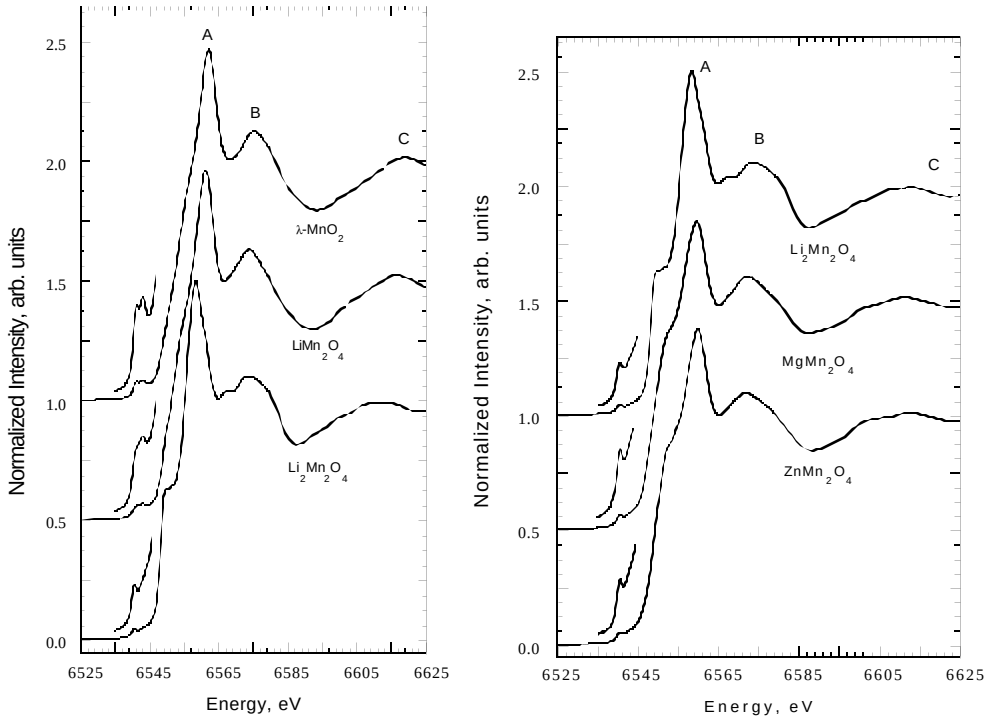

Figure 2. (right) Normalized XANES of $LiMn_2O_4$ along with chemically prepared λ- MnO_2 and $Li_2Mn_2O_4$. (left) Comparison of XANES from $Li_2Mn_2O_4$ with the tetragonal spinels $ZnMn_2O_4$ & $MgMn_2O_4$. Insets shows magnified view of the pre-edge.

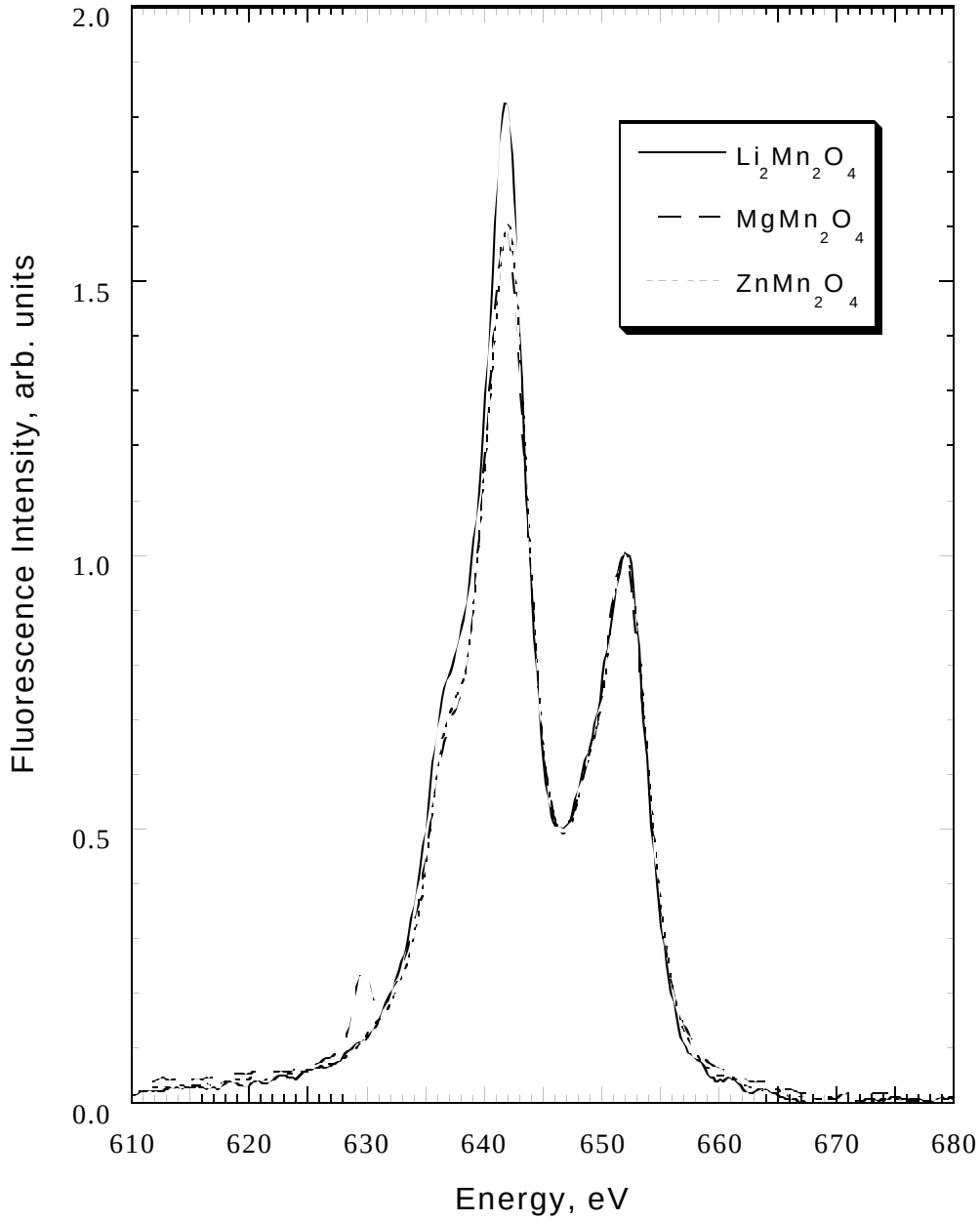

Figure 3. Manganese L-edge XES spectra for $Li_2Mn_2O_4$, $MgMn_2O_4$, and $ZnMn_2O_4$..

* present address: NanoGram Corporation, Fremont, CA 94538

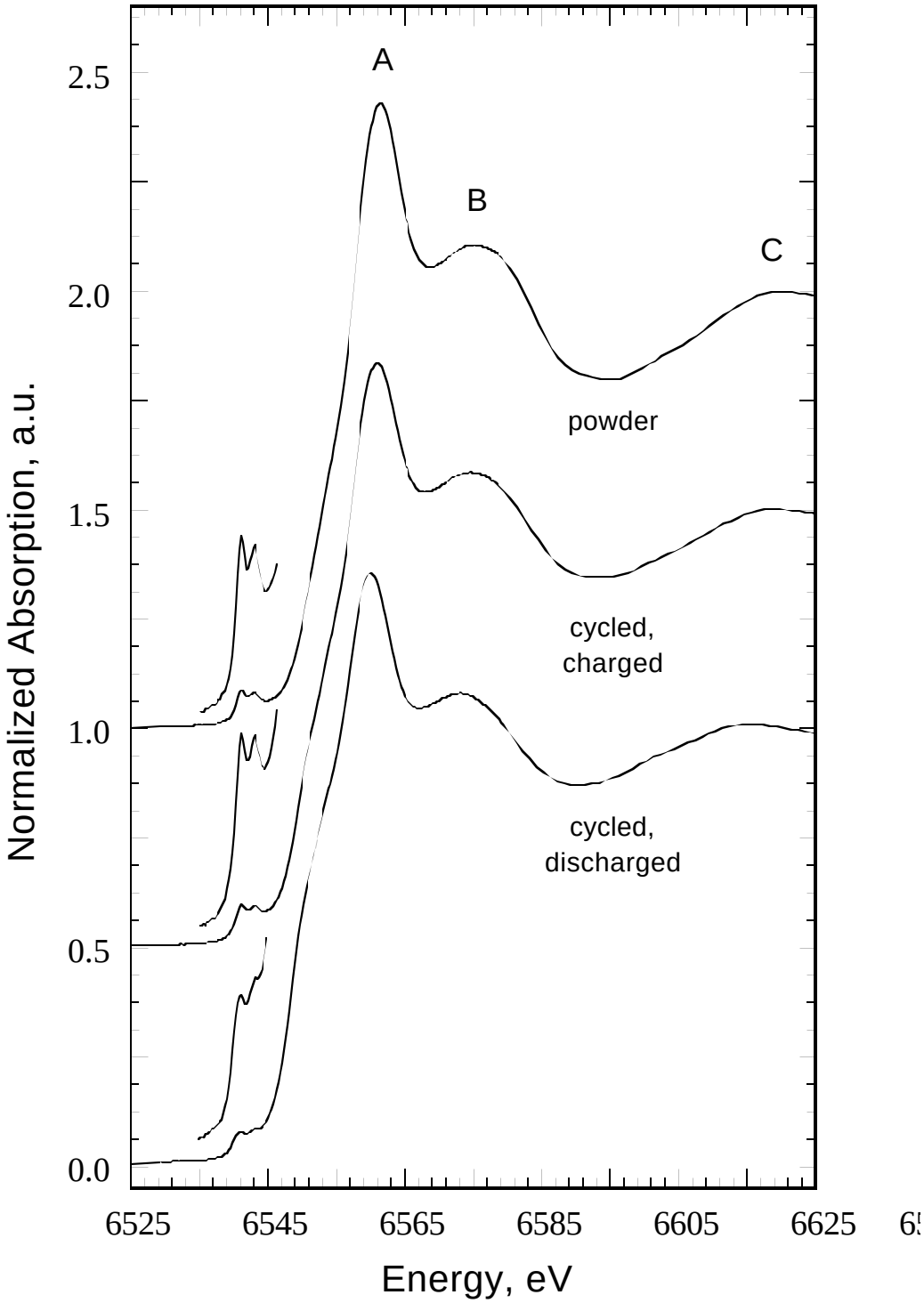

(a) (b)

Figure 4. Mn K-edge XANES from $Li_{1.5}Na_{0.5}MnO_{2.85}I_{0.12}$ (powder), cycled, charged electrode, and cycled discharged electrode.